Physical and chemical evidence for metallofullerenes with metal atoms as part of the cage

David E. Clemmer, Joanna M. Hunter, Konstantin B. Shelimov & Martin F. Jarrold*

Department of Chemistry, Northwestern University, 2145 Sheridan Road, Evanston, Illinois 60208, USA

SINCE the discovery of fullerenes[1], efforts have been made to trap metal atoms inside fullerene cages[2], and both endohedral[3,4] and exohedral[5,6] metallofullerenes have been synthesized. There is, however, a third possibility: a 'networked' metallofullerene, where the metal atom is incorporated into the carbon cage. Here we report the results of experiments to study the structure and reactivity of gas-phase fullerenes doped with niobium (NbC_n^+ with n = 28–50). These experiments, which use injected-ion drift-tube techniques, indicate that for fullerenes containing an even number of carbon atoms the metal is endohedral, but for fullerenes with an odd number of carbon atoms, the niobium metal is bound as a part of the carbon cage. Thus, networked metallofullerenes appear to be a stable class of metallofullerene. We suggest that such metallofullerenes can form if the metal atom retains sufficient electron density to form several strong covalent metal–carbon bonds.

Although boron can be readily networked into fullerene cages[7], evidence for a stable class of networked metallofullerenes is scant[2]. It has been suggested that because the average nearest-neighbour C–C distance in a fullerene is only 1.44 Å, the small boron atom will be the only substitutional dopant, as found for graphite[8]. So far, the only evidence supporting the existence of networked metallofullerenes has been found for a few small LaC_n^+ (n = 31, 33, 35 and 37) clusters where the fullerene cage becomes too small to readily encapsulate the metal, thus squeezing it out of the cage[9]. Here we report physical and chemical studies of the structures of gas-phase NbC_n^+ (n = 28–50) clusters which show that networked metallofullerenes are stable for some metals. The networked structures are formed for clusters containing an odd number of carbon atoms, where the metal atom can occupy the defect site in the fullerene cage that results from the missing carbon atom.

Our injected-ion drift-tube apparatus has been described in detail previously[10]. NbC_n^+ ions generated by pulsed laser vaporization of a mixed NbC/graphite composite rod were size selected by a quadrupole mass spectrometer. Previous unsuccessful attempts at producing NbC_n^+ clusters have been interpreted as an indication that NbC_n^+ metallofullerenes are unstable[11]. We were unable to observe NbC_n^+ clusters with a Nb:C ratio of 1:60, but they form readily when the ratio is 1:10. Pulses (25- or 50-μs) of mass-selected NbC_n^+ ions were injected (at an energy of 150 eV) into a drift tube containing helium. Drift-time distributions were collected under room temperature conditions (~300 K and ~5 torr), and with the drift tube cooled using liquid nitrogen (~77 K and ~2.1 torr). The drift time (the time required for the ions to travel across the drift tube) depends on the average collision cross-section, such that isomers with compact geometries have shorter drift times than ones with less compact geometries. This was first demonstrated for organic ions by Hagen using ion mobility spectrometry[12]. von Helden *et al.* were the first to apply this idea to atomic-cluster ions using injected-ion drift-tube techniques[13,14]. The room temperature conditions are used so that we can easily compare the mobilities measured here to ones measured previously[9,13,14]. The cold conditions are used to enhance the resolution[15–17]. On entering the drift tube, the ions experience a rapid transient heating cycle as their kinetic energy is thermalized by collisions with the buffer gas[18]. This causes some annealing but almost no dissociation (less than 10%). After leaving the drift tube, the ions are focused into a second quadrupole mass spectrometer that is used to monitor fragmentation and transmit only the ion of interest.

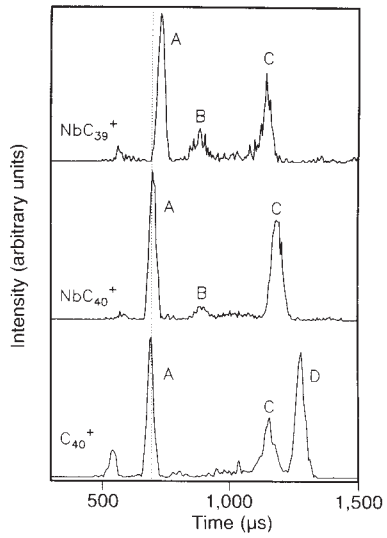

FIG. 1 Drift-time distributions recorded for C_{40}^+ (bottom), NbC_{40}^+ (middle) and NbC_{39}^+ (top) at 77 K and 2.070(±0.005) torr. The drift tube is 7.62 cm long and the drift field was 13.12 V cm^{-1}. Isomers A, B and C have been assigned to fullerene, graphitic sheets and bicyclic ring isomers, respectively (see text). Isomer D corresponds to a monocyclic carbon ring. The dotted line shows that the C_{40}^+ and NbC_{40}^+ fullerenes have nearly identical drift times, suggesting that the metal is inside the fullerene cage. The drift time for NbC_{39}^+ is substantially longer, suggesting that NbC_{39}^+ is not an endohedral metallofullerene.

Figure 1 shows the drift-time distributions recorded for NbC_{39}^+, NbC_{40}^+ and C_{40}^+ at 77 K. For C_{40}^+, the peaks labelled A, C and D have been previously assigned to the fullerene, bicyclic ring and monocyclic ring isomer, respectively[13,14]. Peak A for NbC_{40}^+ occurs at essentially the same time as peak A for C_{40}^+, indicating that the former species is an endohedral metallofullerene. The most striking feature of the data in Fig. 1 is that the NbC_{39}^+ fullerene isomer has a longer drift time than the NbC_{40}^+ and C_{40}^+ fullerenes, even though this cluster contains fewer carbon atoms. This behaviour is observed for all of the neighbouring even-numbered (NbC_{2n}^+ or C_{2n}^+) and odd-numbered (NbC_{2n-1}^+) clusters above NbC_{36}^+. For NbC_n^+ with $n \leqslant 36$, peak A always occurs at longer times than for the analogous C_n^+ cluster. Peaks B and C in the NbC_n^+ drift-time distributions are assigned to graphitic sheets and bicyclic rings containing niobium and will be discussed elsewhere (D.E.C. and M.F.J., manuscript in preparation). Monocyclic rings, an important isomer for pure carbon clusters (peak D), are not observed for NbC_n^+ clusters in this size range.

Figure 2 shows the inverse reduced (normalized to 273 K and 760 torr) mobilities for C_n^+, LaC_n^+ and NbC_n^+ fullerenes determined from drift-time distributions collected at ~300 K and ~5 torr. As discussed previously[9], the mobilities of LaC_{34}^+, LaC_{36}^+ and larger clusters are essentially identical to those measured for the corresponding C_n^+ fullerenes, indicating that they are endohedral metallofullerenes. LaC_{37}^+, LaC_{35}^+ and smaller LaC_n^+ fullerenes have inverse mobilities that are substantially larger than their corresponding C_n^+ fullerenes. For these clusters, calculated inverse mobilities for model metallofullerene structures show that the lanthanum is either exohedral or networked[9]. The measured mobilities for NbC_{37}^+ and smaller niobium metallofullerenes show similar behaviour to the small

* To whom correspondence should be addressed.

LaC_n^+ clusters, indicating a non-endohedral geometry due to the metal atom being squeezed out of the cage. But for the larger NbC_n^+ clusters, only those with an even number of carbon atoms form endohedral metallofullerenes. The larger odd-numbered NbC_n^+ clusters have inverse mobilities that are substantially greater than their C_n^+ analogues, indicating that the metal atom is not encapsulated within the carbon cage.

To test this idea further, we have studied the chemical reactivity of C_n^+ and NbC_n^+ clusters with O_2 and N_2 at 300 K. For these experiments, partial pressures of 0.002–0.008 torr of either O_2 or N_2 were added to the He buffer gas. Mass spectra and drift-time distributions were then collected to investigate the chemical reactivity of the NbC_n^+ clusters. All of the isomers displayed in Fig. 1 for pure C_n^+ clusters (over the entire 30–50 atom range) are unreactive towards both O_2 and N_2 at reagent partial pressures of up to 0.008 torr. Under these conditions, NbC_n^+ clusters react with oxygen to form $NbC_n(O)_x^+$ ($x=1$–5); they react with nitrogen primarily by forming NbC_n^+–(N_2) and to a much lesser degree NbC_n^+–$(N_2)_2$ (<10% of total product formation). Figure 3 shows the reactivity results recorded for NbC_{39}^+ and NbC_{40}^+ with N_2 at a partial pressure of ~0.002 torr. These data have been normalized and scaled by the measured fraction of the unreacted parent ions, such that the peaks in the drift-time distributions represent the abundance of each NbC_{39}^+ and NbC_{40}^+ isomer that remains after the clusters have passed through the drift tube. Clearly the NbC_{39}^+ fullerene isomer reacts with N_2 whereas the NbC_{40}^+ fullerene is essentially inert. When the same fraction of O_2 is added to the He buffer gas, no reaction is observed for the NbC_{40}^+ fullerene whereas the NbC_{39}^+ fullerene reacts away entirely. Results comparable to those for NbC_{40}^+ are observed for NbC_{38}^+ and larger NbC_{2n}^+ clusters. All NbC_{2n-1}^+ clusters, and NbC_{2n} fullerenes that contain fewer than 38 carbons, show substantial reactivity towards both reagent gases, as was observed for NbC_{39}^+. These results indicate that the Nb atom is responsible for the observed reactivity, and that for NbC_{2n-1}^+ fullerenes, the metal is accessible at the surface of the cage.

The results presented here show clearly that the niobium atom is trapped inside even-numbered carbon cages (having at least

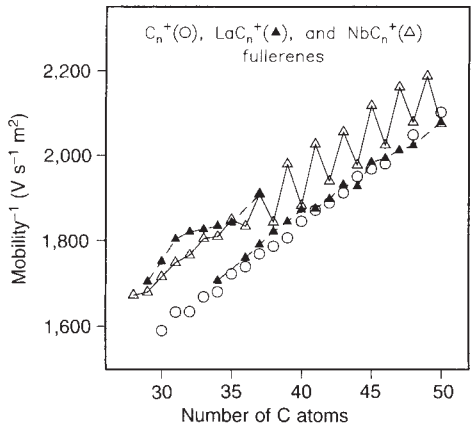

FIG. 2 Inverse reduced mobilities for the fullerene isomers (determined from data taken at ~300 K and ~5.0 torr) plotted against the number of carbon atoms in the cluster for C_n^+ (open circles), LaC_n^+ (solid triangles) and NbC_n^+ (open triangles). The inverse mobilities for LaC_{29}^+–LaC_{35}^+ and LaC_{37}^+ are 9–12% larger than the inverse mobilities for the pure C_n^+ clusters; this indicates that lanthanum is attached to the outside surface of the fullerene. The mobilities for LaC_{36}^+, LaC_{38}^+ and larger LaC_n^+ are essentially identical to those measured for C_n^+, indicating that the metal is endohedral. In the niobium system, NbC_{38}^+ and larger NbC_{2n}^+ clusters have inverse mobilities that indicate that they are endohedral metallofullerenes. All of the NbC_{2n-1}^+ fullerenes, as well as NbC_{36}^+ and smaller NbC_{2n}^+ metallofullerenes, have mobilities that imply an isomer where the metal is attached to the outside surface of the fullerene.

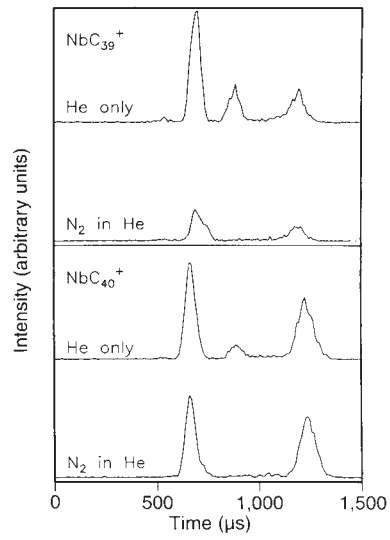

FIG. 3 Drift-time distributions for NbC_{39}^+ (top two traces) and NbC_{40}^+ (bottom two traces) in pure He and in a mixture of N_2 in He (see text). Isomer B, the graphitic sheet, reacts away completely for both NbC_{39}^+ and NbC_{40}^+. Isomers A and C (the fullerene and bicyclic ring isomers, respectively) are substantially more reactive for NbC_{39}^+ than for NbC_{40}^+. The low reactivity of the bicyclic ring (isomer C) for NbC_{2n}^+ is consistent with a geometry where the Nb atom is tetrahedrally coordinated by insertion into two orthogonal carbon rings (D.E.C. and M.F.J., unpublished results).

38 atoms) but resides at the surface of carbon clusters containing odd numbers of carbon atoms. The only reasonable explanation for the results for NbC_{2n-1}^+ fullerenes is that the metal can substitute for the missing carbon atom in an odd-numbered fullerene cage, stabilizing the resulting NbC_{2n-1}^+ metallofullerene. Our quantum-chemical calculations (using the Gaussian 92 program, Gaussian Inc., Pittsburgh) show that the resulting networked structures have a fairly distorted geometry—the metal atom sits outside the surface of the carbon shell—because the Nb–C bonds are significantly longer than C–C bonds (~2.0 Å for NbC compared to ~1.4 Å for carbon).

Insight into why niobium networks into large carbon cages, rather than being trapped inside (as observed for lanthanum) can be gained by considering the Nb^+ and La^+ ions. Nb^+ has four valence electrons and should bond strongly with the sp^2-hybridized carbon atoms in the fullerene cage. La^+ has only two valence electrons and therefore cannot thoroughly satisfy the four-electron hole at the cage defect. Furthermore, electron paramagnetic resonance (EPR)[19] and theoretical[20,21] studies show that La^{3+} is found within fullerenes, further weakening the metal's ability to contribute covalently to the carbon framework. Thus the La^{3+} which resides on the inside of the fullerene cage is stabilized by ionic interactions with the negatively charged fullerene cage. On the other hand, the first and second ionization energies of Nb atoms (6.88 eV and 14.32 eV, respectively)[22] are significantly larger than those of La atoms (5.577 eV and 11.06 eV)[22]. It therefore seems likely that Nb^+ will retain more of its valence electron density, enabling it to form covalent bonds with the four electrons at the defect site and network at the surfaces of even very large C_{2n-1}^+ cages. Indeed, our quantum-chemical calculations for networked NbC_{29}^+ and LaC_{29}^+ fullerenes determine a Mulliken charge of +1 on Nb and +2 on La, consistent with these simple arguments.

The preference of large even-numbered NbC_{2n}^+ clusters to form endohedral metallofullerenes can be understood by considering the energetic differences between carbon–carbon and metal–carbon covalent bonds. Thermochemistry for metal–carbon systems shows that the bond energies of even the strongest metal–

carbon single and double bonds (~2.5 eV and 4.1 eV, respectively)[23] are much weaker than carbon–carbon single and double bonds (~3.8 eV and 7.5 eV, respectively)[22]. Thus although the ionic interactions between lanthanum and the inside of a fullerene cage discussed above are probably weaker for niobium, the large energy difference between the formation of C–C and Nb–C bonds favours the all-carbon cage rather than the metal-substituted cage for NbC_{2n}^{+} metallofullerenes.

Our results show that networked metallofullerenes are a stable class of metallofullerene for some metals. In addition to the results for niobium described here, we have recently obtained preliminary evidence indicating that some of the larger zirconium-containing fullerenes are networked. Because the metal atom is exposed in a networked metallofullerene, these species may possess catalytic properties as well as large dipoles and useful optical properties. They may self-assemble into novel layered materials. It should be possible to attach inorganic ligands during or immediately after production, which would not only provide a rational scheme for further stabilizing these species, but might also lead to extraction and purification procedures that use the metal–ligand chemistry. We are currently attempting to synthesize macroscopic quantities of these materials along these lines so that their properties can be examined in detail. □

Received 18 August; accepted 12 October 1994.

1. Kroto, H., Heath, J. R., O'Brien, S. C., Curl, R. F. & Smalley, R. E. *Nature* **318,** 162–163 (1985).
2. Bethune, D. S., Johnson, R. D., Salem, J. R., de Vries, M. S. & Yannoni, C. S. *Nature* **366,** 123–128 (1993).
3. Weiss, F. D., O'Brien, S. C., Elkind, J. L., Curl, R. F. & Smalley, R. E. *J. Am. chem. Soc.* **110,** 4464–4465 (1988).
4. Chai, Y. *et al. J. phys. Chem.* **95,** 7564–7568 (1991).
5. Roth, L. M. *et al. J. Am. chem. Soc.* **113,** 6298–6299 (1991).
6. McElvany, S. W. *J. phys. Chem.* **96,** 4935–4937 (1992).
7. Guo, T., Jin, C. & Smalley, R. E. *J. phys. Chem.* **95,** 4948–4950 (1991).
8. Dresselhaus, M. S., Dresselhaus, G. & Eklund, P. C. in *Encyclopedia of Applied Physics* Vol 6,515–544 (VCH, Weinheim, Germany, 1992).
9. Shelimov, K. S., Clemmer, D. E. & Jarrold, M. F. *J. phys. Chem.* (in press).
10. Jarrold, M. F., Bower, J. E. & Creegan, K. *J. chem. Phys.* **90,** 3615–3628 (1989).
11. Guo, T., Smalley, R. E. & Scuseria, G. E. *J. chem. Phys.* **99,** 352–359 (1993).
12. Hagen, D. F. *Analyt. Chem.* **51,** 870–874 (1979).
13. von Helden, G., Hsu, M.-T., Kemper, P. R. & Bowers, M. T. *J. chem. Phys.* **95,** 3835–3837 (1991).
14. von Helden, G., Hsu, M.-T., Gotts, N. & Bowers, M. T. *J. phys. Chem.* **97,** 8182–8192 (1993).
15. Rivercomb, H. E. & Mason, E. A. *Analyt. Chem.* **47,** 970–983 (1975).
16. Rokushika, S., Hatano, H., Baim, M. A. & Hill, H. H. *Analyt. Chem.* **57,** 1902–1907 (1985).
17. Kemper, P. R. & Bowers, M. T. *J. phys. Chem.* **95,** 5134–5146 (1991).
18. Jarrold, M. F. & Honea, E. C. *J. phys. Chem.* **95,** 9181–9185 (1991).
19. Johnson, R. D., de Vries, M. S., Salem, J. R., Bethune, D. S. & Yannoni, C. S. *Nature* **355,** 239–240 (1992).
20. Laasonen, K., Andreoni, W. & Parrinello, M. *Science* **258,** 1916–1918 (1992).
21. Nagase, S., Kobayashi, K., Kato, T. & Achiba, Y. *Chem. Phys. Lett.* **201,** 475–480 (1993).
22. Weast, R. C. (ed.) *CRC Handbook of Chemistry and Physics* 63rd edn (CRC, Boca Raton, Florida, 1982).
23. Armentrout, P. B. & Georgiadis, R. *Polyhedron* **7,** 1573–1581 (1988).

ACKNOWLEDGEMENTS. We thank R. Hudgins for his help in collecting some of the reactivity data. This work was supported by the US NSF and the Petroleum Research Fund (administered by the American Chemical Society).

Effect of precipitation on the albedo susceptibility of clouds in the marine boundary layer

Robert Pincus & Marcia B. Baker

Geophysics Program AK-50, University of Washington, Seattle, Washington 98195, USA

TROPOSPHERIC aerosols are thought to have three important effects on the Earth's radiation budget: the direct radiative effect[1] (perturbation of clear-sky reflectivity), the indirect radiative effect[2] (modification of cloud albedo) and the effect on the hydrological cycle[3] (modification of the vertical thickness and horizontal extent of clouds). The first two effects have been understood in principle for nearly 20 years, and quantitative estimates of their magnitudes have been provided by models and observations[4]. The third phenomenon, and its relation to the other two, has received far less attention. Previous work[3] has shown, however, that increases in aerosol concentration may act to increase cloud albedo by increasing horizontal cloud fraction as well as cloud reflectivity. Here we use a simple model of the marine cloud-topped boundary layer to investigate the changes in cloud thickness and albedo that result from changes in precipitation as particle concentrations vary. We find that the sensitivity of layer cloud albedo to droplet number concentration (the albedo susceptibility) is increased by 50–200% when the dependence of cloud thickness on particle number is included. The results suggest that the response of cloud thickness to changes in aerosol particle concentration must be taken into account for accurate prediction of global albedo by climate models.

Aerosols affect cloud properties by acting as cloud condensation nuclei (CCN) upon which cloud droplets form. An increase in droplet number concentration N (cm^{-3}) at constant liquid-water mixing ratio q_l (kg water per kg air) results in a decrease in the average droplet radius and an increase in total droplet surface area and cloud albedo A. The effect can be quite large—an order-of-magnitude change in N can induce relative changes in A as large as 30% (ref. 5). This process is often quantified in terms of albedo susceptibility[6]:

$$S_0 \equiv \left.\frac{\partial A}{\partial N}\right|_{q_l} \qquad (1)$$

Measurements from satellites[7] and aircraft[8] of marine boundary-layer clouds around the world show that susceptibility varies widely under natural circumstances, and indicate that anthro-

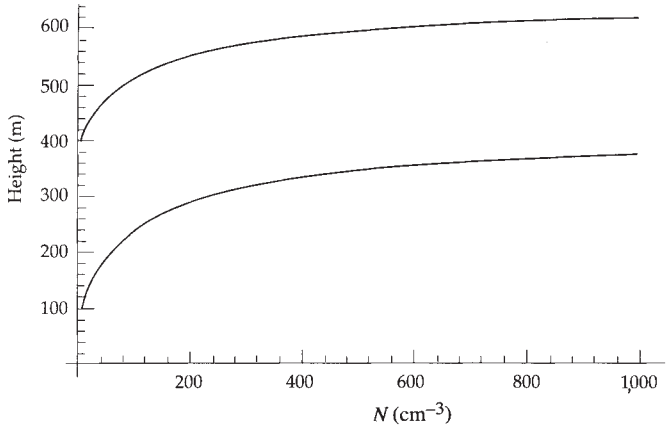

FIG. 1 Predicted equilibrium cloud thickness h (bottom trace) and cloud-top height z_i (top trace) as functions of droplet concentration N. Increases in N lead to decreases in the average cloud droplet radius and so to decreases in precipitation. This affects the boundary-layer energy budget, causing entrainment to increase and z_i to rise. Cloud thickness is most sensitive to changes in droplet concentrations when droplet concentrations are low. Droplet concentrations of 10 cm^{-3} have been observed in the Southern Hemisphere; concentrations of 1,000 cm^{-3} represent highly polluted air from continental sources. The predictions arise from a mixed-layer model of the marine boundary layer which includes parametrizations of radiation and precipitation.